A Wireless In-Flight Charging Range Extended PT-WPT System Using S/Single-Inductor-Double-Capacitor Compensation Network for Drones

Yu Gu, *Student Member, IEEE*, Jiang Wang, *Member, IEEE*, Zhenyan Liang, *Member, IEEE*, and Zhen Zhang, *Senior Member, IEEE*

***Abstract*—To address the special challenges for drone wireless in-flight charging systems, namely the continuous fluctuation of mutual inductance, large charging distance, and limited payload of the pickup, a novel high-order primary-series (S) and secondary-single-inductor-double-capacitor (SLDC) topology for parity-time (PT) symmetric wireless power transfer (WPT) system is proposed in this article. The reduced-order model of the proposed system is first established and analyzed based on the coupled-mode theory. It shows the critical coupling coefficient can be reduced by two additional degrees of freedom (λ and L_r), thus effectively expanding the constant power (CP) region of PT-WPT system. In addition, the inductor L_r can be placed freely in drones and λ can be flexibly adjusted to meet the demands of various environments, which enhance the system flexibility. Also, the communication link and dc–dc converter are not needed, which improve the real time and reduce the drone payload. Simulated and experimental results prove that the transfer distance can be extended by 102% with $\lambda = 0.6$ and $L_r = 60.5\ \mu$H while keeping the CP of 75 W and efficiency of 87.5% against the misalignment and change of the charging distance. Accordingly, with the proposed S/SLDC topology, drone in-flight charging systems can obtain a larger CP region with high efficiency, thus extending the flight time of drones.**

***Index Terms*—Drone, in-flight charging, parity-time (PT) symmetry, S/single-inductor-double-capacitor (SLDC) topology, wireless power transfer (WPT).**

I. Introduction

SINCE drones can perform tasks with their advantages of flexibility and intelligence in complex working conditions, they have gained widespread attention from business and academia. It is forecasted that the global drone market will reach US$ 55.8 billion by 2026 at 7.8% compound annual growth rate (CAGR), with the commercial market growing at 8.3% [1]. As the biggest limitation of drones, the flight time, which is commonly half an hour, needs to be greatly extended to meet various requirements. Fortunately, wireless power transfer (WPT) provides a revolutionary means for the fast charging of drones with the outstanding superiority [2], [3]. Especially for the remote and harsh environment (no landing platform), the in-flight charging technology [4], [5] offers an innovative approach for wireless charging of drones, which can theoretically extend the flight time to infinity. Besides, the in-flight drones can perform line monitoring tasks with their large shooting distance and angle of view while charging, whereas this technology brings a special challenge: How to maintain the constant charging power for the drone lithium batteries under the large range of continuous fluctuation of mutual inductance?

To overcome the effect of mutual inductance on the output characteristics of the WPT system, various methods have been proposed, which mainly include coil structure design [6], [7]; parameter estimation [8]; impedance transformation network [9]; and parity-time (PT) symmetric theory [10], [11]. In [6], a novel design method for the reversed-series compensation coil structure is proposed to improve the misalignment tolerance, and another dual transmitters and dual receivers with integrated decoupling coils is introduced in [7] with a good misalignment performance, whereas the above coil structures with ferrites may be not suitable for the drone in-flight charging system since the ferrites will increase the weight of the pickup and reduce in-flight time of drones. Besides, the mutual-inductance-dynamic-predicted control was proposed to avoid the effect of mutual inductance for in-flight charging of drones with high prediction accuracy [8]. But the model-based control method may fail due to large parameter perturbations. In [9], a serial/parallel capacitor matrix was designed to automatically track the impedance-matching point against the varying distance. Moreover, a concept of PT symmetry from the quantum physics has been applied to the WPT system [10], which has attracted significant attention due to its special features of constant output power and efficiency against the mutual inductance.

In comparison with other control schemes against mutual inductance, the novel WPT system based on PT symmetry can realize the automatic frequency regulation to maintain constant

Manuscript received 28 March 2023; revised 18 June 2023; accepted 8 July 2023. Date of publication 17 July 2023; date of current version 1 September 2023. This work was supported by the National Natural Science Foundation of China under Grant 51977138. Recommended for publication by Associate Editor Mahshid Amirabadi. *(Corresponding author: Zhen Zhang.)*

The authors are with the School of Electrical and Information Engineering, Tianjin University, Tianjin 300072, China (e-mail: guyu1997@tju.edu.cn; jiangwang@tju.edu.cn; liangzy@tju.edu.cn; zhangz@tju.edu.cn).

Color versions of one or more figures in this article are available at https://doi.org/10.1109/TPEL.2023.3294485.

Digital Object Identifier 10.1109/TPEL.2023.3294485

power (CP). The control circuit is implemented on the primary side without wireless communication, which improves the real-time performance and reduces the payload of pickup. However, only when the coupling coefficient κ is higher than a certain value, namely in the exact PT-symmetric region, the CP can be obtained. Otherwise, in the case of weak coupling, the output power and efficiency will still be influenced by the change of relative position between the transmitting and pickup coils. In consequence, the CP region of the PT-WPT system is necessary to be expanded, namely achieving the longer transfer distance, which can satisfy the needs of different application situations.

Currently, some common methods, such as repeater coil [12], [13], magnetic materials [14], and parameter optimization [15], can be used to extend the transfer distance of the WPT system. In [13], the PT-based WPT system with multirepeater (odd and even number of repeaters) was proposed to extend the transfer distance with the reduction of the critical coupling coefficient, whereas mutual inductances from the repeater to the transmitting and pickup coils are required to be identical, which is hard to implement for some applications. In addition, while magnetic materials such as ferrites facilitate the enhancement of mutual inductance [14], the resulting magnetic loss and increased weight in the WPT system should be considered along with the extended distance. With the increase in the self-inductance of the pickup coil, the critical coupling of the PT-WPT system can be reduced [15], thus expanding the CP region. But this will result in the increases in size and weight of the pickup, which will be limited by the space and payload of the charging devices.

Moreover, different from other WPT applications (electric vehicles (EVs) [16], autonomous underwater vehicle (AUV) [17], and consumer electronics [18], [19]), the in-flight charging system of drones faces the greater practical challenges, including the large range of continuous fluctuation of mutual inductance and the limited payload of drones. First, there is a certain distance between the in-flight drones and the charging tower for safe charging, which may lead to the weak coupling of the WPT system. Meanwhile, in-flight drones will fluctuate frequently by the environmental influence, thus resulting in large and continuous changes of mutual inductance. Accordingly, the robust charging power is required against the mutual inductance with a larger transfer distance. Besides, the limited payload of drones requires as little unnecessary weight as possible on the pickup, which can reduce the power losses of in-flight drones.

To address the above issues, the novel primary-series (S) and secondary-single-inductor-double-capacitor (SLDC) topology for the PT-based WPT system is proposed in this article, which can greatly expand and adjust the exact PT-symmetric region (CP range) of the PT-WPT system with high misalignment tolerance and high system flexibility. Specifically, the main contributions of the proposed system can be summarized as follows.

1) Based on the coupled-mode theory (CMT), the proposed S/SLDC PT-WPT system is first built with the reduced-order model to facilitate analysis. Compared with the common S/S topology, the proposed system can obtain a much larger exact PT-symmetric region with two additional degrees of freedom. Thus, the robust CP range with high misalignment tolerance can be greatly expanded to meet a wide range of charging demand.

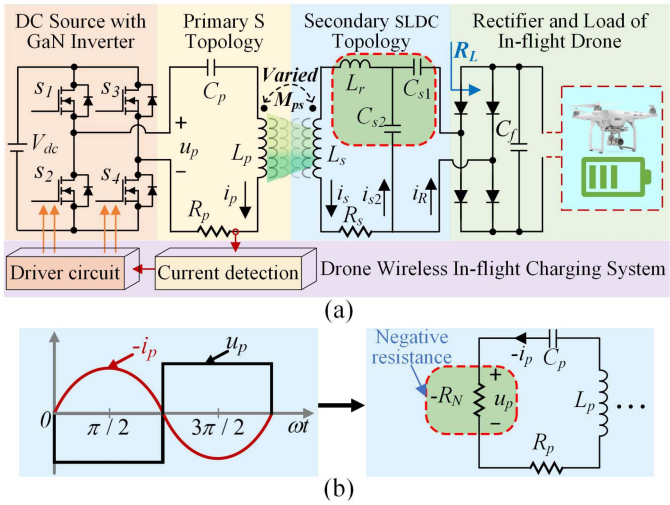

Fig. 1. Schematic of (a) drone wireless in-flight charging system with the proposed S/SLDC topology based on PT-symmetric principle and (b) the negative resistance $-R_N$ for the proposed PT-WPT system.

2) The parameter design process for the proposed system has been introduced, which shows the high system flexibility with the added degrees of freedom (λ and L_r). It can easily and simply regulate the suitable CP region with high transfer efficiency to satisfy the meet for various types of drones and environments.
3) The sensor and control are on the primary side without the wireless communication and dc–dc converter on the pickup. In addition, the proposed S/SLDC topology will not add much space or weight of the pickup due to the small size inductor L_r and capacitor of the same total value C_s. Hence, the proposed system can guarantee the lightweight design of pickup on drones.

II. System Analysis and Modeling

Fig. 1(a) depicts the drone wireless in-flight charging system with the high-order S/SLDC compensation topology, in which S_1–S_4 constitute a full-bridge inverter, L_p, L_s, and M_{ps} are the self-inductances of transmitting and pickup coils and the mutual inductance between them. L_r is the inductance of the inductor added to the pickup side circuit. C_p, C_{s1}, and C_{s2} are the compensation capacitors of inductors. R_L represents the equivalent resistance of drone battery R_{dro} after rectification and filtering, where $R_L = 8R_{dro}/\pi^2$. R_p is the internal resistance of inductance L_p, and R_s is the sum internal resistances of inductances L_s and L_r. $V_{\rm dc}$ is the input dc voltage. In the proposed PT-WPT system, the system input voltage u_p is controlled to be in the opposite phase of the input current $-i_p$. Hence, the dc source with inverter can be viewed as a negative resistance $-R_N$, as shown in Fig. 1(b).

To facilitate the analysis of the energy transfer between coupled resonators, the CMT model of the PT-WPT system is adopted in this article. It should be noted that the high-order compensation capacitors C_{s1} and C_{s2} can be further simplified as the compensation capacitor C_s based on the equivalent circuit method, which is conducive to the establishment of coupled

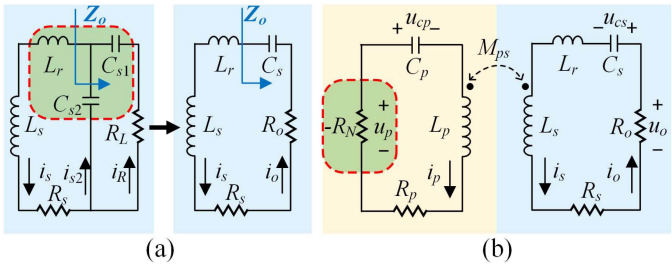

Fig. 2. (a) Equivalent transformation of the secondary-SLDC topology. (b) Simplified equivalent circuit of the proposed PT-WPT system.

mode equations. As shown in Fig. 2(a), the equivalent output impedance Z_o can be expressed as

$$Z_o = \frac{1}{j\omega C_s} + R_o = \frac{1}{j\omega C_{s2}} // \left(\frac{1}{j\omega C_{s1}} + R_L\right) = \frac{\left[C_{s1} + C_{s2} + \omega^2 C_{s1}^2 C_{s2} R_L^2\right]/(j\omega) + C_{s1}^2 R_L}{(C_{s1} + C_{s2})^2 + \omega^2 C_{s1}^2 C_{s2}^2 R_L^2}. \quad (1)$$

In the normal PT-based WPT system, it can be satisfied that $\omega^2 C_{s1}^2 C_{s2}^2 R_L^2 << (C_{s1} + C_{s2})^2$ and $\omega^2 C_{s1}^2 C_{s2} R_L^2 << C_{s1} C_{s2}$. Thus, with the simplification of (1), it can be obtained as

$$\begin{cases} C_s = C_{s1} + C_{s2} \\ R_o = \frac{C_{s1}^2 R_L}{(C_{s1}+C_{s2})^2} = \lambda^2 R_L. \end{cases} \quad (2)$$

Here, define $\lambda = C_{s1}/(C_{s1}+C_{s2})$ as the capacitance ratio on a scale of 0 to 1. C_s and R_o are the equivalent compensation capacitor and equivalent load resistance, respectively. Based on the equivalent transformation, the high-order SLDC topology of the pickup can be reduced as *LC*-transformed topology. Fig. 2(b) depicts the equivalent circuit of the proposed high-order S/SLDC PT-based WPT system. Based on Fig. 2(b), the circuit equations of the proposed system can be expressed as

$$\begin{cases} L_p \frac{di_p}{dt} + M_{ps} \frac{di_s}{dt} + u_{cp} + i_p R_p = u_p \\ M_{ps} \frac{di_p}{dt} + (L_s + L_r) \frac{di_s}{dt} + u_{cs} + i_s (R_s + R_o) = 0 \\ C_p \frac{du_{cp}}{dt} = i_p \\ C_s \frac{du_{cs}}{dt} = i_s. \end{cases} \quad (3)$$

Here, i_p, i_s, and i_o denote the currents flowing through L_p, L_s, and R_o, respectively. u_{cp} and u_{cs} represent the voltages of the coils L_p and L_s, respectively. Based on the fundamental harmonics approximation method, the inverter output voltage u_p satisfies that $u_p = 4V_{\mathrm{dc}}/(\sqrt{2}\pi)$. According to the CMT model [20], the energy modes ψ_p and ψ_s of the transmitting and pickup resonators can be described as

$$\begin{cases} \psi_p = \Psi_p e^{j(\omega t + \theta_p)} = \sqrt{\frac{L_p}{2}} i_p + j\sqrt{\frac{C_p}{2}} u_{cp} \\ \psi_s = \Psi_s e^{j(\omega t + \theta_s)} = \sqrt{\frac{L_s + L_r}{2}} i_s + j\sqrt{\frac{C_s}{2}} u_{cs} \end{cases} \quad (4)$$

where ω is the system operating angular frequency, Ψ_p and Ψ_s are the amplitudes of the energy modes, and θ_p and θ_s are the corresponding phases. Then, the circuit state variables of the WPT system can be expressed in the energy model as

$$\begin{cases} i_p = \Psi_p \sqrt{\frac{2}{L_p}} \cos(\omega t + \theta_p) \\ u_{cp} = \Psi_p \sqrt{\frac{2}{C_p}} \sin(\omega t + \theta_p) \\ i_s = \Psi_s \sqrt{\frac{2}{L_s + L_r}} \cos(\omega t + \theta_s) \\ u_{cs} = \Psi_s \sqrt{\frac{2}{C_s}} \sin(\omega t + \theta_s). \end{cases} \quad (5)$$

It should be noted that the natural resonant frequencies of transmitting and pickup resonators are denoted as $\omega_p = 1/\sqrt{L_p C_p}$ and $\omega_s = 1/\sqrt{(L_s + L_r) C_s}$, respectively. And the PT-symmetric WPT system should satisfy $\omega_p = \omega_s = \omega_0$. Then, based on (5), the dynamics of the coupled modes can be derived, and the detailed theoretical derivation is carried out in the Appendix.

It is assumed that the amplitudes and phases of the energy modes are constant during a switching period, and the high-frequency terms can be eliminated based on the averaging method [21]. Thus, the dynamic equations can be described as

$$\frac{d}{dt}\begin{bmatrix} \psi_p \\ \psi_s \end{bmatrix} = \begin{bmatrix} j\omega_0 + \frac{1}{\Psi_p}\frac{2V_{\mathrm{dc}}}{\pi\sqrt{2L_p}} - \frac{R_p}{2L_p} & -j\kappa'\frac{\omega_0}{2} \\ -j\kappa'\frac{\omega_0}{2} & j\omega_0 - \frac{R_s+R_o}{2(L_s+L_r)} \end{bmatrix} \begin{bmatrix} \psi_p \\ \psi_s \end{bmatrix} \quad (6)$$

where the coupling coefficient between transmitter and pickup is $\kappa = M_{ps}/\sqrt{L_p L_s}$ and the equivalent coupling coefficient of the proposed system is $\kappa' = M_{ps}/\sqrt{L_p(L_s + L_r)}$. Based on (6), the frequency characteristic equation of the system can be obtained as

$$\begin{vmatrix} j(\omega_0 - \omega) + \frac{1}{\Psi_p}\frac{2V_{\mathrm{dc}}}{\pi\sqrt{2L_p}} - \frac{R_p}{2L_p} & -j\kappa'\frac{\omega_0}{2} \\ -j\kappa'\frac{\omega_0}{2} & j(\omega_0 - \omega) - \frac{R_s+R_o}{2(L_s+L_r)} \end{vmatrix} = 0. \quad (7)$$

With the separation of the real and imaginary parts of the characteristic equation, (7) can be expressed as

$$\begin{cases} \frac{\kappa'^2\omega_0^2}{4} - (\omega - \omega_0)^2 + \left(\frac{R_p}{2L_p} - \frac{1}{\Psi_p}\frac{2V_{\mathrm{dc}}}{\pi\sqrt{2L_p}}\right) \times \frac{R_s+R_o}{2(L_s+L_r)} = 0 \\ (\omega - \omega_0)\left(\frac{1}{\Psi_p}\frac{2V_{\mathrm{dc}}}{\pi\sqrt{2L_p}} - \frac{R_p}{2L_p} - \frac{R_s+R_o}{2(L_s+L_r)}\right) = 0. \end{cases} \quad (8)$$

Then, the steady solution of the operation frequency ω is derived as (9), and the amplitudes of the energy modes in the proposed system can be expressed as (10)

$$\omega = \omega_{1,2} = \omega_0 \pm \sqrt{\left(\frac{\kappa'\omega_0}{2}\right)^2 - \left[\frac{R_s + R_o}{2(L_s + L_r)}\right]^2} \quad (9)$$

$$\Psi_p = \Psi_s = \frac{2\sqrt{2L_p}(L_s + L_r) V_{dc}}{\pi\left[R_p(L_s + L_r) + (R_s + R_o) L_p\right]}. \quad (10)$$

According to (9), when the operation frequency $\omega = \omega_0$, the critical coupling coefficient κ_c of the proposed S/SLDC PT-based WPT system can be calculated and obtained as (11). When $\kappa \geq \kappa_c$, the system operates in the exact PT-symmetric region [22]. In contrast, the system will enter the broken PT-symmetric region, whose output characteristics are identical to the normal

TABLE I
COMPARISON BETWEEN THE PERFORMANCE OF THE PROPOSED SYSTEM AND THE SS PT-SYMMETRIC SYSTEM

	The proposed system	The SS PT-symmetric system
Critical coupling coefficient	$\frac{R_s+\lambda^2 R_L}{\omega_0\sqrt{L_s(L_s+L_r)}}$	$\frac{R_s+R_L}{\omega_0 L_s}$
Output power	$\frac{8V_{dc}^2\lambda^2 R_L L_p(L_s+L_r)/\pi^2}{\left[R_p(L_s+L_r)+(R_s+\lambda^2 R_L)L_p\right]^2}$	$\frac{8V_{dc}^2 R_L L_p L_s/\pi^2}{\left[R_p L_s+(R_s+R_L)L_p\right]^2}$
Transfer efficiency	$\frac{\lambda^2 R_L}{R_p(L_s+L_r)/L_p+R_s+\lambda^2 R_L}$	$\frac{R_L}{R_p L_s/L_p+R_s+R_L}$

WPT system with the fixed operation frequency ω_0

$$\kappa_c=\frac{R_s+R_o}{\omega_0\sqrt{L_s(L_s+L_r)}}=\frac{R_s+\lambda^2 R_L}{\omega_0\sqrt{L_s(L_s+L_r)}}. \tag{11}$$

Significantly, the critical coupling coefficient κ_c of the proposed system is mainly determined by the natural resonant frequency ω_0, capacitance ratio λ, load R_L, pickup coil L_s, and added resonator L_r. The capacitance ratio λ and resonator L_r are two additional degrees of freedom of the S/SLDC topology, which can be easily and flexibly designed to reduce the value of κ_c. With the reduction of κ_c, the proposed S/SLDC PT-WPT system can greatly expand the exact PT-symmetric region to ensure a wide range of constant output characteristics as follows.

In the exact PT-symmetric region, based on (9) and (10), the system operating frequency can automatically stabilize at $\omega_{1,2}$ rather than ω_0, which will change with the coupling coefficient κ. Meanwhile, the output power P_{out} and transfer efficiency η of the proposed system can be obtained as

$$P_{\text{out}}=\frac{R_o\Psi_s^2}{L_s+L_r}=\frac{8V_{\text{dc}}^2 R_o L_p(L_s+L_r)}{\pi^2[R_p(L_s+L_r)+(R_s+R_o)L_p]^2} \tag{12}$$

$$\eta=\frac{R_o\Psi_s^2/(L_s+L_r)}{R_p\Psi_p^2/L_p+(R_s+R_o)\Psi_s^2/(L_s+L_r)}=\frac{R_o}{R_p(L_s+L_r)/L_p+R_s+R_o}. \tag{13}$$

It can be found from (12) and (13) that both the output power and transfer efficiency of the proposed system are independent of the coupling coefficient κ in the exact PT-symmetric region, which can also be seen from Fig. 9. Moreover, the comparison between the output performance of the proposed S/SLDC PT-WPT system and the S/S PT-WPT system is listed in Table I. It can be seen that compared with the S/S topology, the critical coupling coefficient of the proposed system will be reduced with λ and L_r, thus expanding the CP region. Meanwhile, the output power and efficiency can keep constant against mutual inductance in the exact PT-symmetric region. Thus, with the proposed system, the expanded CP charging range for drones can be got regardless of the large and continuous fluctuation of transfer distance between charging tower and in-flight drones, which effectively improves the system stability and adaptability.

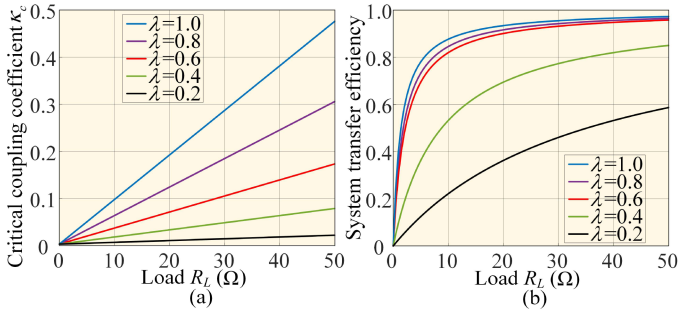

Fig. 3. (a) Critical coupling coefficient κ_c and (b) efficiency η versus load R_L with different capacitance ratios λ in the proposed system.

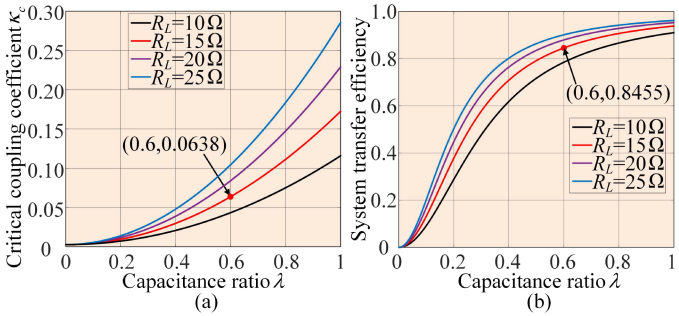

Fig. 4. (a) Critical coupling coefficient κ_c and (b) efficiency η versus capacitance ratio λ with different loads R_L in the proposed system.

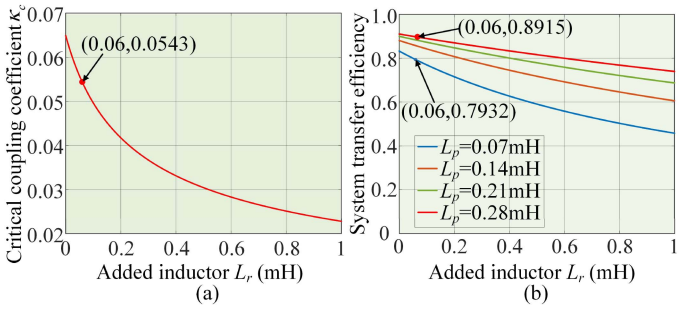

Fig. 5. (a) Critical coupling coefficient versus added inductor L_r. (b) Efficiency η versus L_r with different L_p in the proposed system.

III. SYSTEM IMPLEMENTATION

A. System Output Characteristics

Based on the above analysis in Section II, the proposed S/SLDC PT-based WPT system has two additional degrees of freedom (capacitance ratio λ and added resonator L_r) compared with the common S/S topology, which can be flexibly designed to reduce the critical coupling coefficient. Though the decrease of κ_c can expand the CP region of PT-WPT system, the system efficiency η will be affected by λ and L_r at the same time, which should be considered. Thus, to optimize the proposed system, the influences of key system parameters on the critical coupling coefficient κ_c and transfer efficiency η are analyzed in the following and the corresponding curves are shown in Figs. 3–5, which can be used to guide the parameter design of the proposed topology.

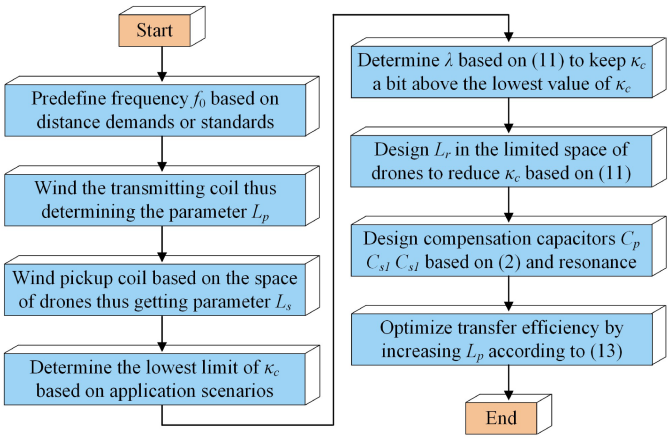

Fig. 6. Flowchart of parameter design.

Based on (11) and (13), when the transmitting and pickup coils are determined, the critical coupling coefficient κ_c and the efficiency η are mainly related to the load R_L, capacitance ratio λ, and added inductor L_r. The corresponding curves against the load R_L are shown in Fig. 3, which shows that the larger load will lead to a high transfer efficiency with a large value of λ. In this article, the load is selected as 15 Ω for further analysis of the system output characteristics. As can be observed from Fig. 4, the critical coupling κ_c decreases with the reduction of λ, but the transfer efficiency η will decrease at the same time. Besides, as the added inductor L_r increases, the critical coupling κ_c will reduce accompanied by a decrease in efficiency as shown in Fig. 5. Hence, the appropriate λ and L_r should be chosen to extend the PT-symmetric range while taking into account both critical coupling coefficient and system efficiency.

The flowchart of parameter design is shown in Fig. 6. First, the natural resonant frequency f_0 is selected based on the transfer distance requirement and standard for operation frequency. In addition, the transmitting and pickup coils can be prewound to determine the values of L_p and L_s. It is worth noting that the transmitting coil can be added with ferrite to enhance the magnetic coupling strength. But the pickup coil requires to be as light as possible to reduce payload on the drone, so ferrite needs to be avoided. Then, the minimum coupling between the coupling coils obtained from experimental tests is used as the expected critical coupling κ_{c_exp}, thus ensuring that the PT-WPT system is always in the exact region. Subsequently, capacitance ratio λ can be selected based on (11) to keep κ_c a bit larger than the expected value of κ_{c_exp}. Moreover, the added inductor L_r is wound and determined to reduce the value of κ_c to below the expected value, which should consider the limited space of drones. According to (2) and resonant state, capacitors C_p, C_{s1}, C_{s1} are calculated and designed. Based on (13), the value of L_p can improve the transfer efficiency without sacrificing critical coupling κ_c. Therefore, if necessary, the value of L_p can be increased to optimize efficiency. An illustration is given in the following.

For exemplification, when $f_p = f_s = 100$ kHz, $L_p = 73.5$ μH, $L_s = 140$ μH, $R_p = 0.39$ Ω, $R_s = 0.24$ Ω, $R_L = 15$ Ω, the critical coupling coefficient of SS PT-symmetric system (as Case 1) is 0.1724. To reduce the value of κ_c below 0.06, the capacitance ratio λ, which has a huge impact on κ_c, is first selected as 0.6. Then, the value of κ_c is reduced to 0.0638. Meanwhile, it can be found from Fig. 5(a) that κ_c decreases at a greater rate when the added inductor L_r is less than 200 μH. When L_r is larger, the increase in L_r has little effect on κ_c. Thus, to maximize the benefits of L_r on the reduction of κ_c, L_r is suggested to be less than 200 μH. Here the inductance L_r is set 60.5 μH. When the parameters λ and L_r of the proposed system are determined (as Case 2), κ_c has been decreased to 0.0543 as expected. It should be noted that although the proposed system greatly extends the PT-symmetric range with the reduction of κ_c (from 0.1724 to 0.0543), the system efficiency of Case 2 is only 79.32%. Significantly, as shown in Fig. 5(b), the larger transmitting inductance L_p will improve the system efficiency, and the critical coupling κ_c will remain unchanged based on (11). Thus, to maintain high transmission efficiency, L_p is increased to 280 μH (as Case 3) with the efficiency of 89.15% to meet design requirements. Finally, the system output characteristics (output power, transfer efficiency, and operating frequency) of Cases 1–3 are compared as shown in Fig. 9. In conclusion, the proposed S/SLDC PT-based WPT system can effectively expand the CP region with the high efficiency.

Furthermore, the extra degrees of freedom (λ and L_r) can be flexibly and conveniently designed to meet various demands of the CP range expansion for drone in-flight charging systems. To be specific, the sum of C_{s1} and C_{s2} in the proposed system is equal to the compensation capacitor C_s of the pickup inductor for the common PT-WPT system and λ is the capacitance ratio of C_{s1}, which facilitates the parameter design and modification. Besides, the added inductor L_r has the advantages of relatively small size, light weight, and freedom of placement. In the confined space of drones, the added inductor can be placed flexibly to make the most of the space at the pickup end as it does not need to be coupled to the transmitting coil.

B. Negative Resistance Design

To realize the proposed PT-WPT system, the inverter output voltage u_p is controlled to be in the opposite phase to current $-i_p$, which is viewed as a negative resistance. Here, the phase synchronization method based on digital signal processor (DSP) controller is used to realize the negative resistance. As shown in Fig. 7(a), the phase and frequency of primary current i_p are detected with the detection circuit, which are sent to the controller with the generation of the complementary inverter switching signals. Then, the inverter output voltage u_p is generated, with its phase 180° from i_p.

The detailed scheme of the controller is shown in Fig. 7(b). First, i_p is detected by the current sensor, and the square wave u'_p in phase with i_p is obtained by passing through the low pass filter respectively (LPF) and zero-crossing comparator. LPF is used to overcome the disruption of stray signal interference or ringing. Then, the frequency and phase information are recognized by the eCAP module of DSP. Finally, the pulsewidth modulation signal is generated in the DSP and sent to the gate driver, which ensures the phase difference between i_p and u_p. Based on the above control scheme, the

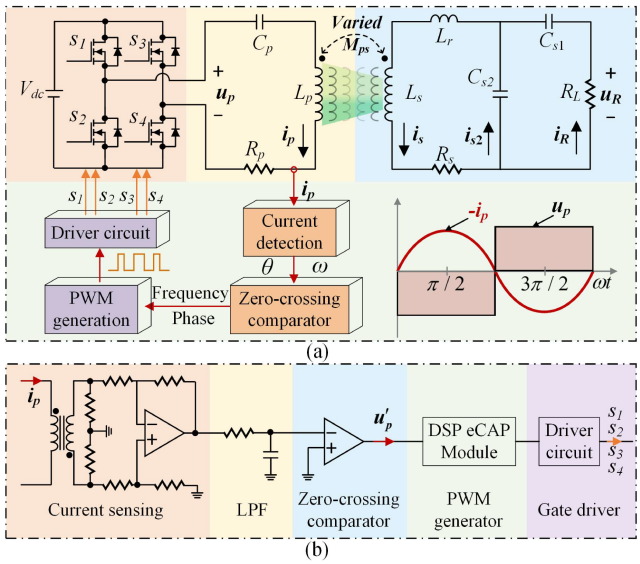

Fig. 7. (a) Block diagram of the proposed S/SLDC PT-based WPT system. (b) Signal processing circuit for the negative resistance $-R_N$.

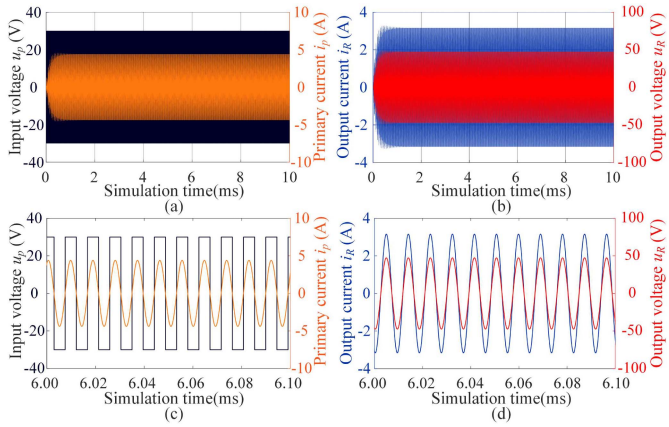

Fig. 8. Simulated results of the proposed system in Case 3, where $\kappa = 0.2$. (a) Startup process with u_p and i_p. (b) Startup process with i_R and u_R. (c) u_p and i_p after zooming in. (d) i_R and u_R after zooming in.

operation frequency will automatically stabilize at $\omega_{1,2}$ with the change of mutual inductance in the exact PT-symmetric region [22]. Then, the constant output power and transfer efficiency can be obtained. Besides, the proposed PT-WPT system can be easily selected to operate at high frequency (ω_1) or low frequency (ω_2) as long as the value of the period register PRD is limited to be less or greater than PRD_0 ($\mathrm{PRD}_0 = 2\pi/(\omega_0 \mathrm{T_{CLK}})$, $\mathrm{T_{CLK}}$ is the time required for the counter to increment by 1). Here, the low frequency is selected as the operating frequency to reduce the switching and conduction loss of switching devices in inverters to improve efficiency. Compared with other control schemes, the whole detection and control are set up on the primary side, which will not increase the payload of drones, thus extending the in-flight time of drones.

IV. Simulation

To verify the proposed S/SLDC PT-based WPT system, the simulation model based on MATLAB/Simulink is established with the key parameters in Table I, which includes three cases of PT-WPT system. Case 1 is the common S/S topology, where $L_p = 73.5\ \mu$H, $L_s = 140.7\ \mu$H, $R_p = 0.39\ \Omega$, and $R_s = 0.24\ \Omega$. To expand the CP region, Case 2 of the proposed S/SLDC topology with added λ and L_r is designed, where $L_p = 73.5\ \mu$H, $L_s = 140.7\ \mu$H, $R_s = 0.34\ \Omega$, $L_r = 60.5\ \mu$H, and $\lambda = 0.6$. Moreover, to keep the CP range expansion with the high efficiency, Case 3 only increases the transmitting inductance of Case 2, where $L_p = 285.1\ \mu$H and $R_p = 0.45\ \Omega$.

Fig. 8 shows the simulated waveforms of voltage and current in the proposed S/SLDC PT-WPT system with $\kappa = 0.2$, which shows that the proposed system can quickly reach the steady state. Meanwhile, the inverter voltage and current are controlled to be in phase with the operating frequency of 109.32 kHz. Besides, the output current and power are 2.23 A and 74.59 W,

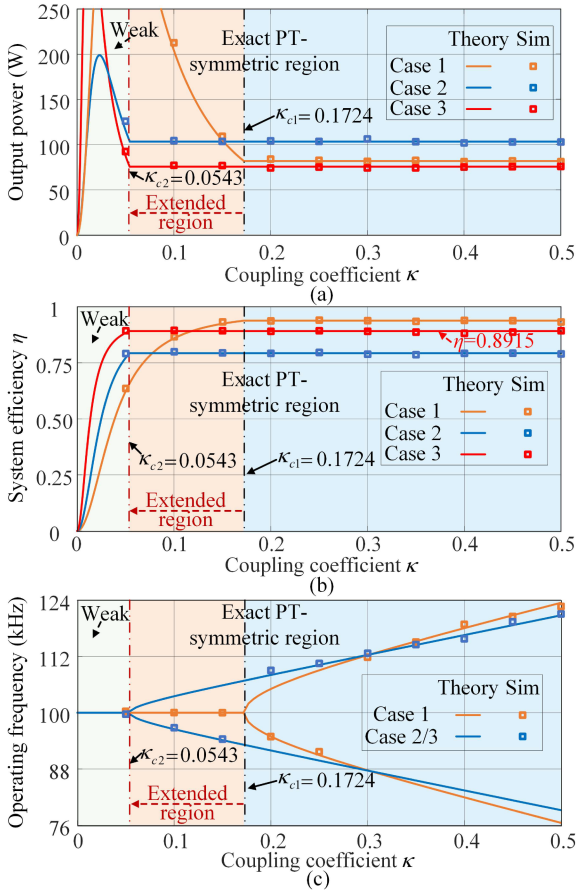

Fig. 9. Theoretical and simulated results in Cases 1–3. (a) Charging power with different κ. (b) Transfer efficiency with different κ. (c) Operating frequency with different κ.

which can prove the CP feature of the proposed system as shown in Fig. 9.

Furthermore, to compare the system output characteristics, the theoretical and simulated results in Cases 1–3 are depicted in Fig. 9, which include the output power, transfer efficiency,

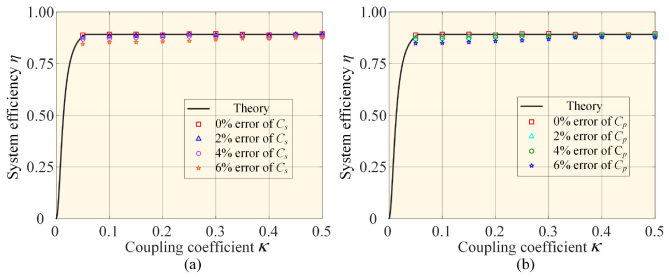

Fig. 10. System efficiency under different coupling coefficient κ with respect to the fluctuation of (a) C_s and (b) C_p.

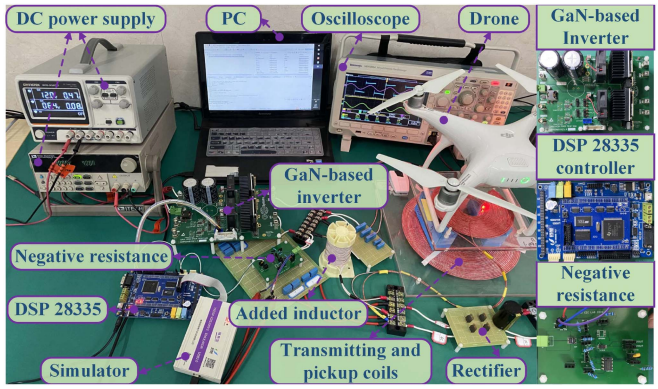

Fig. 11. Experimental prototype.

and operating frequency. It is observed that the critical coupling coefficient κ_c is reduced from 0.1724 to 0.0543 with the proposed system. Besides, the increase of L_p improves the system efficiency to 89.15% without affecting the value of κ_c. The simulation results prove the expansion capability of the CP region of the proposed system with high efficiency, which can be applied for the drone wireless in-flight charging system to meet the demands of the large-distance CP charging range.

In practical charging system for drones, the parameters of the energy storage components including inductors and capacitors may change slightly. The component tolerances will lead the natural resonant frequency to shift, which will cause the detuning of the WPT system. Taking Case 3 for instance, the sensitivity analysis of the proposed S-SLDC PT-WPT system is studied. To simulate the frequency detuning ($\omega_p \neq \omega_s$), the compensation capacitance (C_s/C_p) of the transmitting/pickup side is adjusted to deviate a little from the resonance value, respectively. (The parameter deviations of inductors will have a similar effect on system detuning.) Fig. 10 shows the transfer efficiency under different coupling coefficients when the values of parameters C_s/C_p deviate by 0%, 2%, 4%, and 6%. It can be observed that the acceptable component error of the proposed system is about 4%, which has a little effect on the system. In addition, the similar limit of component tolerances is also mentioned in [10] for the WPT system. Moreover, the selection of the polypropylene capacitors and the parallel connection of multiple capacitors can help to reduce the capacitor error and thus decreasing the frequency detuning of the WPT system.

V. Experiment

A. Experimental Results of the Proposed System

As shown in Fig. 11, the experimental prototype is established to validate the feasibility of the proposed S/SLDC PT-based WPT system, where the system parameters are in Table II. The high-frequency ac voltage of the WPT system is offered by the power supply (Itech IT6722A) and the GaN-based full-bridge inverter (GSP65R13HB-EVB). The rectifier bridge adopts the fast recovery epitaxial diode (DSEI 2x 30-12B) with low losses and short recovery time. In the control circuit, the current sensor adopts CU8965 and the operational amplifier selects LM6172. After passing through the LPF and zero-crossing comparator, the frequency and phase of primary current i_p are captured by the DSP. The oscilloscope (MDO3024) is used to analyze and display the experimental waveforms. In addition, the litz wire (Φ: 0.1 mm $\times$ 200 strands) is tightly wound to make the coils, the capacitors adopt polypropylene capacitors with low tolerance and high voltage resistance, and the loads select RF resistors.

TABLE II
Key Parameters of Prototype

Item	Value
Inductance of transmitting coil (L_p)	73.5/285.1 μH
Resistance of primary side (R_p)	0.39/0.45 Ω
Capacitance of primary side (C_p)	34.47/8.89 nF
Inductance of pickup coil (L_s)	140.7 μH
Inductance of added inductor (L_r)	60.5 μH
Capacitance of series capacitor (C_{s1})	7.55 nF
Capacitance of parallel capacitor (C_{s2})	5.04 nF
Resistance of secondary side (R_s)	0.34 Ω
Resistance of load (R_L)	15 Ω
System natural operating frequency (f_0)	100 kHz

Fig. 12(a) shows the measured coupling coefficients between the transmitting and pickup coils at different transfer distances. Here, the yellow area represents the exact PT-symmetric region of the common S/S topology with the critical coupling 0.1724, where the maximum transfer distance is 85 mm. The green area represents the expanded exact PT-symmetric region with the proposed S/SLDC topology, where κ_c is reduced to 0.0543 and the maximum transfer distance is prolonged to 172 mm. Also, the measured coupling coefficients under different transmission distances and lateral misalignments are depicted by the three-dimensional grid diagram in Fig. 12(b), which can cover the common range for the drone in-flight charging system. It is clear to observe that the CP region (namely exact PT-symmetric region) of PT-WPT system is greatly expanded with the proposed S/SLDC topology. In addition, it is considered that both the lateral and angular misalignments between the transmitting and pickup coil may occur in the drone in-flight charging system. Then, to verify the misalignment tolerance characteristics of the proposed system, the related measured values of κ are shown in Fig. 13, where the blue area is the extended CP region with the proposed topology. In short, the experimental results can verify

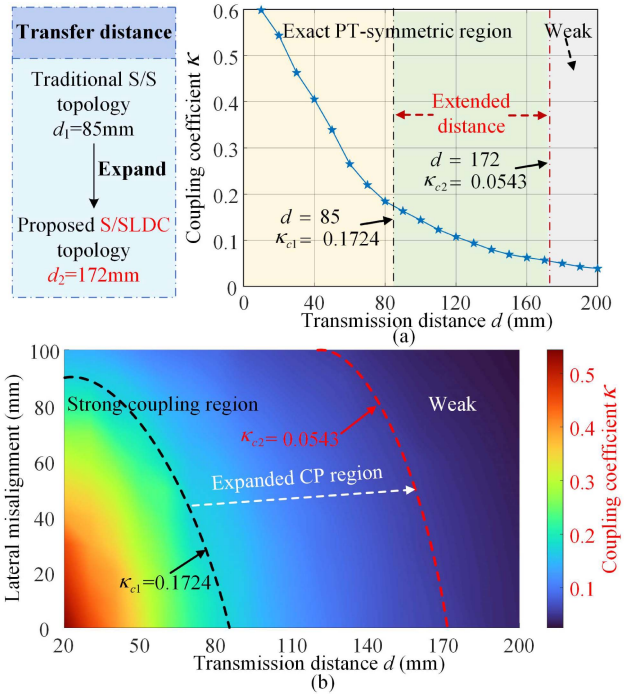

Fig. 12. Experimental results of the coupling coefficient κ between the transmitting and pickup coils (a) at different transmission distances and (b) at different transmission distances and lateral misalignments.

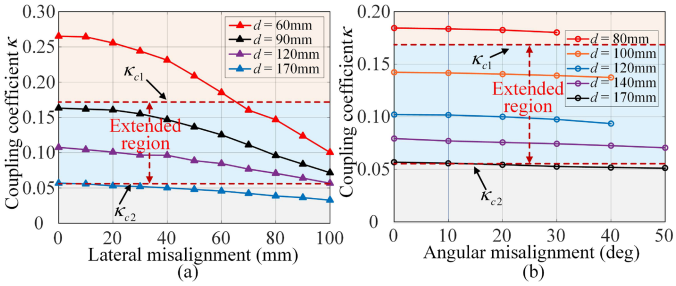

Fig. 13. Experimental results of the coupling coefficient κ (a) versus lateral misalignments with different transmission distances and (b) versus angular misalignments with different transmission distances.

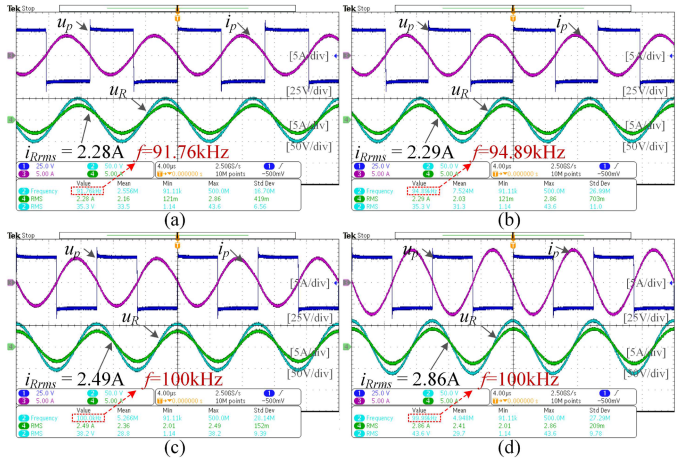

Fig. 14. Experimental waveforms of Case 1 (S/S topology) at different distances d. (a) d = 60 mm. (b) d = 80 mm. (c) d = 100 mm. (d) d = 120 mm.

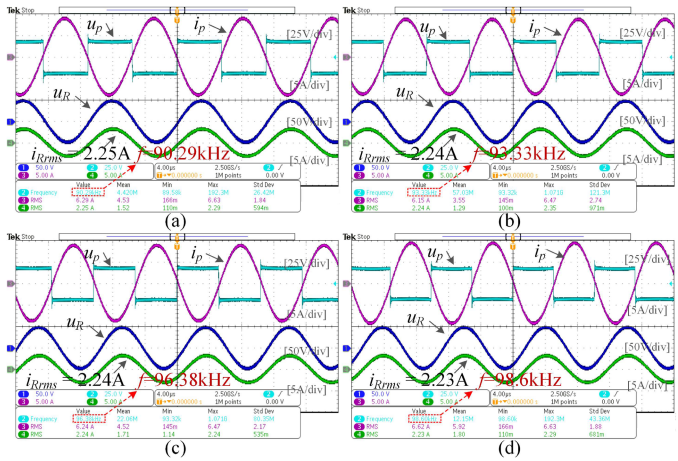

Fig. 15. Experimental waveforms of Case 2 (the proposed S/SLDC topology) at different distances d. (a) d = 60 mm. (b) d = 90 mm. (c) d = 120 mm. (d) d = 170 mm.

the CP range expansion of the proposed S/SLDC compensated PT-WPT system, which is conducive to the long-distance wireless charging for in-flight drones.

The experimental waveforms of the common S/S PT-WPT system (Case 1) under different distances are shown in Fig. 14, where the inverter output voltage and current are in opposite phases. It can be found that the output current keeps unchanged at about 2.3 A in d = 60 mm and d = 80 mm, where the system is in the exact PT region. The output power and transfer efficiency are 79.4 W and 91.82%, respectively. Then, when the transfer distance increases to 100 and 120 mm, the output current increases a lot with the fixed frequency of 100 kHz. It reflects the limitations of the conventional topology and the CP region needs to be expanded.

In contrast, the experimental waveforms of the proposed S/SLDC PT-WPT system (Cases 2 and 3) under different transfer distances are shown in Figs. 15 and 16, respectively. In different transfer distances (60, 90, 120, 170 mm) of Case 2, the output current is invariable with the constant output power of 75 W and changed operating frequency, which validates the output robustness of the proposed system. In Case 2, the transfer efficiency is about 77.52%, which can be improved in Case 3. In addition, Fig. 16 also verifies the constant output current can be kept against the transmission distance (90, 120, 160 mm) with and without the rectifier. In Case 3, the output power and efficiency without the rectifier are about 75.26 W and 87.58%, respectively. It can be easily judged that the proposed system works in the exact PT-symmetric state with the constant output power as shown in Figs. 15 and 16, which validates the practicability of the proposed system for the drone wireless in-flight charging.

Moreover, to further compare the output characteristic of the proposed system and the common PT system, the output power P_{out}, transfer efficiency η, and operating frequency f of Cases 1 and 3 are shown in Figs. 17–19. It can be clearly found from

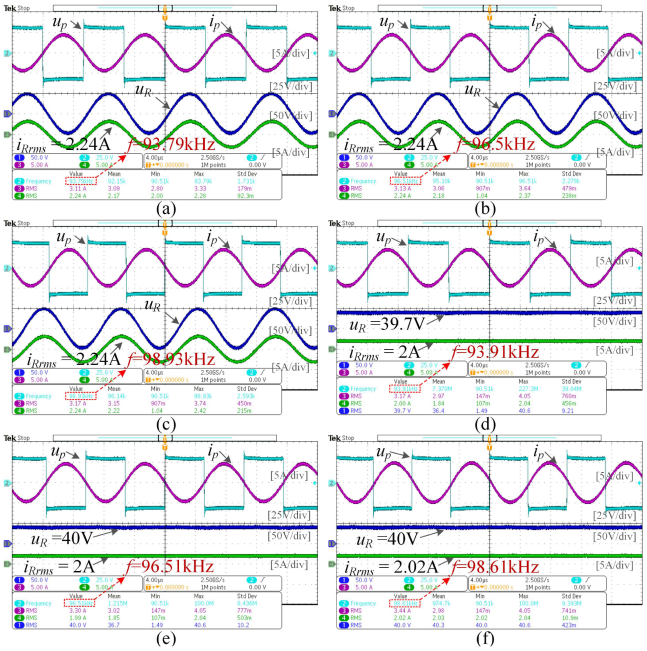

Fig. 16. Experimental waveforms of Case 3 (the proposed S/SLDC topology) at different distances d. (a) $d = 90$ mm. (b) $d = 120$ mm. (c) $d = 160$ mm. (d) $d = 90$ mm with rectifier. (e) $d = 120$ mm with rectifier. (f) $d = 160$ mm with rectifier.

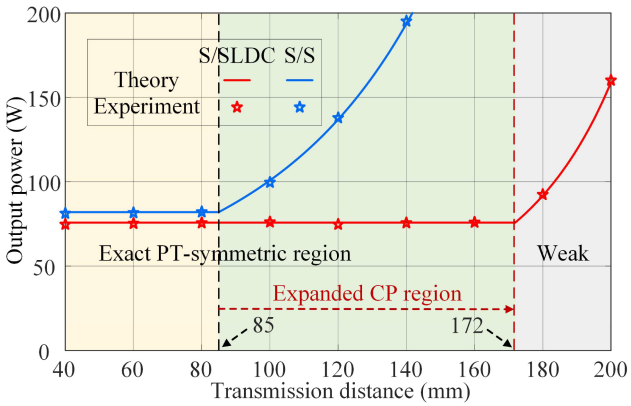

Fig. 17. Comparison of measured and theoretical output power versus transmission distance using the proposed S/SLDC and S/S topology.

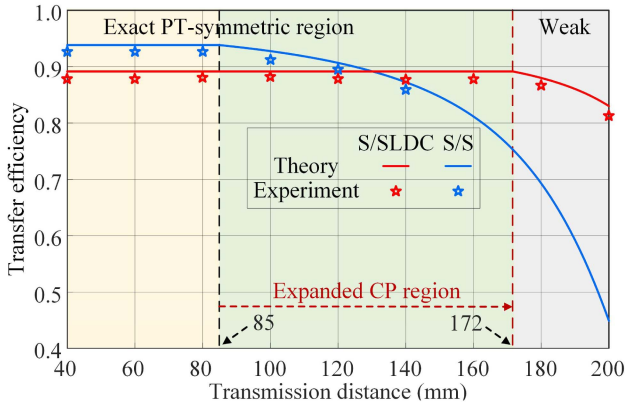

Fig. 18. Comparison of measured and theoretical transfer efficiency versus transfer distance using the proposed S/SLDC and S/S topology.

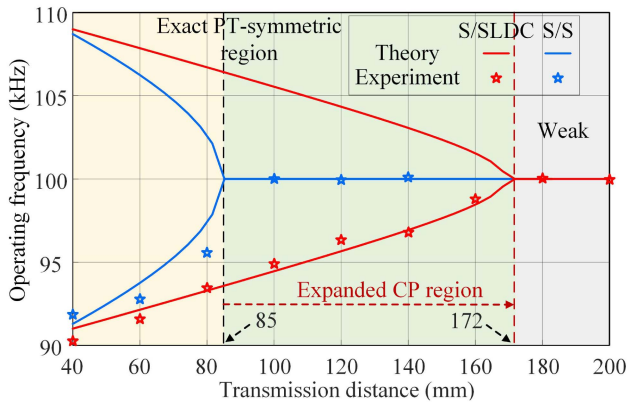

Fig. 19. Comparison of measured and theoretical operating frequency versus transfer distance using the proposed S/SLDC and S/S topology.

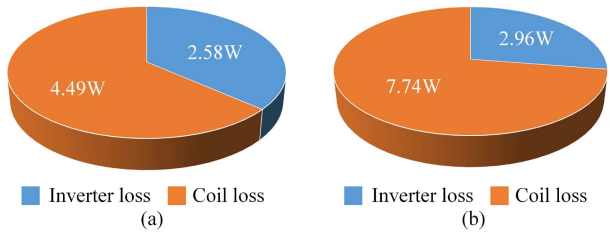

Fig. 20. Power losses of the PT-WPT system with (a) S/S topology and (b) the proposed S/SLDC topology.

Fig. 17 that the proposed S/SLDC topology can maintain the constant output power at around 75 W regardless of the transfer distance. Significantly, the maximum transfer distance has been expanded to 172 mm, which achieves the improvement of 102% over the common topology. Besides, as shown in Fig. 18, the transfer efficiency can stabilize at about 87.5% over a wide CP range of 172 mm, which is the exact PT-symmetric region of the proposed system. In addition, the operating frequency has been verified to be stable at $\omega_{1,2}$ based on (9), as shown in Fig. 19. Accordingly, the proposed system can effectively overcome the frequency splitting phenomenon of the common magnetic resonance-coupled WPT system. In short, the experimental results of the proposed S/SLDC PT-WPT system are essentially close to the theoretical analysis in Section II, namely the CP region can be effectively expanded with the proposed system.

Besides, the power loss analysis of the PT-WPT system is given here, which compares the traditional S/S topology and the proposed high-order S/SLDC topology. In the PT-WPT system, the negative resistance of the article is achieved by controlling the full-bridge inverter. Thus, the loss of the negative resistance is the inverter loss without any other additional loss. In other words, similar to the common inverter loss, the loss of the negative resistance mainly includes the losses of MOSFET. In short, the power losses of the PT-WPT system mainly include the inverter loss and the coil loss, which can be shown in Fig. 20. In the S/S topology, the output power is 79.4 W with the transfer efficiency of 91.82%, and the total power loss is 7.07 W. The coil loss and

TABLE III
COMPARATIVE ANALYSIS BETWEEN THE PROPOSED SYSTEM AND OTHERS

Ref.	Antimisalignment method	Misalignment tolerance /distance expansion ratio	High system flexibility	Meet pickup lightweight?	No wireless communication?	Operating condition	Frequency (MHz)	Distance (mm)	Output power (W)	Transfer efficiency
[3]	Magnetic coupler	Rotation tolerance: 45°	Unexpected	Yes	Yes	Fixed	0.05	100	325	86%
[5]	Control method	Expansion: 50%	Unexpected	No	No	Fixed	0.1	75	25	--
[8]	Control method	Expansion: 37%	Unexpected	Yes	Yes	Fixed	0.2	80	20	82.1%
[22]	Control method	Not mention	Unexpected	Yes	Yes	Variable	1	100	10	93.6%
[23]	Magnetic coupler	Tolerance: 54%	Unexpected	Yes	Yes	Fixed	0.15	50	150	80.6%
[24]	Magnetic coupler	Tolerance: 37%	Good	No	No	Fixed	0.085	--	126	91.6%
[25]	Magnetic coupler	Tolerance: 50%	Unexpected	Yes	Yes	Fixed	0.085	--	135.8	80%
This article	Control method	Expansion: 102%	Good	Yes	Yes	Variable	0.1	172	75	87.5%

the inverter loss are 4.49 and 2.58 W, respectively, with coil loss accounting for a higher proportion of 63.5%. On the other hand, the output power of the proposed S/SLDC topology is about 75 W with the efficiency of 87.5%, and the total power loss is 10.7 W. Among them, the coil loss of 7.74 W accounts for 72.3% of the total loss and the inverter loss of 2.96 W accounts for 27.7%. Although the efficiency of the proposed system has decreased, the decrease does not exceed 5%. More importantly, the transfer distance of the proposed system is about more than twice that of the original S/S PT-symmetric system, which shows a great advantage.

The proposed system can be easily applied for the drone in-flight charging to ensure the constant charging power against the mutual inductance with an expanded long distance. First, the detection and CP control circuits are on the primary side without any extra dc–dc converter and wireless communication, which can guarantee the lightweight design of drones. Besides, two additional degrees of freedom (λ and L_r) can be flexibly designed to regulate the expanded CP region with high transfer efficiency, which can meet the demands of different application scenarios. Meanwhile, the added inductor L_r has the strength of small size and light weight, which can be placed freely in drones since it does not need to be coupled to the transmitting coil.

B. Comparison With Other Drone Charging Systems

To highlight the advantages of the proposed S/SLDC PT-WPT system, Table III compares the characteristics between this work and other drone charging systems recently. The great advantage of the proposed system is the expanded CP charging region with high misalignment tolerance, high system flexibility, and no wireless communication, which is suitable for the drone in-flight wireless charging system.

The antimisalignment method with constant output features for the drone wireless charging mainly includes the magnetic coupler design and various control methods. The magnetic coupler design methods are generally used to obtain a uniform magnetic field distribution by designing a compact and lightweight coupling coil structure, thus improving the system misalignment tolerance [3], [23], [24], [25], whereas they are more suitable for the drone landing charging with a relatively close transfer distance to overcome the effect of landing bias on output characteristics. Compared with [23], [24], and [25], the proposed system in this article can obtain constant charging power with the expanded and large transfer distance, which can be applied in the drone in-flight wireless charging.

In the control methods for the in-flight charging of drones, the dynamic-balancing model-free control [5] was proposed to achieve the constant current output under the change of mutual inductance, and the control method based on mutual inductance prediction [8] was introduced to overcome the effect of mutual inductance. Compared with [5] and [8], the proposed system in this article has high flexibility with two additional degrees of freedom (λ and L_r) to adjust and expand the constant charging power range. Besides, the article and [22] both adopt the PT-based WPT system. In the PT-WPT system, the detection and control circuits are set on the primary side without wireless communication, which improves the real-time performance and reduces the payload of pickup. Compared with the S/S topology in [22], the novel S/SLDC topology proposed in this article can expand the exact PT region with high system flexibility, thus meeting various charging demands of the wide range and long distance. And the frequency can be selected to be low frequency to reduce losses. The comparison of performance parameters is also shown in Table III. It can be observed that the transfer distance with the CP region in this article can reach 172 mm, which is larger than others. Accordingly, the proposed system in this article has competitive advantages due to its large CP region and high flexibility for drone wireless in-flight charging.

VI. CONCLUSION

In the article, a high-order S/SLDC compensated PT-based WPT system with the expanded CP region is proposed for the drone wireless in-flight charging. Based on the CMT model, the theoretical model of the proposed system is built and analyzed, which shows the critical coupling coefficient κ_c can be greatly reduced by added degrees of freedom (λ and L_r). By the design of λ and L_r, the expanded CP range (against mutual inductance) can be obtained. The whole control circuit is on the primary side without the communication link and dc–dc converter, which can improve the system real time and reduce the payload of drones. Besides, the added inductor L_r with a small size can be placed freely in drones and capacitance ratio λ can be flexibly adjusted to balance the output characteristics, which enhances the system flexibility. Simulated and experimental results verify that the charging distance of the proposed system can be expanded by 102% with $\lambda = 0.6$ and $L_r = 60.5$ μH while keeping the CP of 75 W and efficiency of 87.5%. Therefore, the constant charging power with a large range can be ensured for the in-flight drones with the proposed topology, which can enhance the robustness and flexibility of drone in-flight charging system.

Furthermore, the advanced control schemes can be combined with the proposed S/SLDC PT-based WPT system to achieve the regulation of charging power against the load change, which is the focus of future work. In addition, the modulation strategy (such as on–off keying modulation) can help to regulate the equivalent load, hence adjusting the expanded CP region based on (11). It can dynamically and flexibly expand the CP region of the drone charging system without the need to replace the compensation unit, which is also the focus of future research.

APPENDIX

Substituting (5) into (3), the dynamic equations of the CMT model can be derived as (A1) by the averaging method. Based on (4), the derivatives of the energy modes can be obtained as (A2). Then, substituting (A1) into (A2), ignoring the high-order terms, the system equation can be rewritten as (6)

$$\begin{cases} \frac{d\Psi_p}{dt} = \frac{1}{1-k'^2}\left[\frac{2V_{dc}}{\pi\sqrt{2L_p}} - \frac{R_p}{2L_p}\Psi_p + \frac{k'(R_s+R_o)}{2(L_s+L_r)}\right. \\ \quad \left.\times\Psi_s\cos(\theta_p-\theta_s) - \frac{k'\omega_s}{2}\Psi_s\sin(\theta_p-\theta_s)\right] \\ \Psi_p\left(\omega+\frac{d\theta_p}{dt}\right) = \frac{\omega_p}{2}\Psi_p + \frac{1}{1-k'^2}\left[\frac{\omega_p}{2}\Psi_p - \frac{k'\omega_s}{2}\right. \\ \quad \left.\times\Psi_s\cos(\theta_p-\theta_s) - \frac{k'(R_s+R_o)}{2(L_s+L_r)}\Psi_s(\theta_p-\theta_s)\right] \\ \frac{d\Psi_s}{dt} = \frac{1}{1-k'^2}\left[-\frac{2k'V_{\rm dc}}{\pi\sqrt{2L_p}}\cos(\theta_p-\theta_s) - \frac{R_s+R_o}{2(L_s+L_r)}\Psi_s\right. \\ \quad \left.+\frac{k'R_p}{2L_p}\Psi_p\cos(\theta_p-\theta_s) + \frac{k'\omega_p}{2}\Psi_p\sin(\theta_p-\theta_s)\right] \\ \Psi_s\left(\omega+\frac{d\theta_s}{dt}\right) = \frac{\omega_s}{2}\Psi_s + \frac{1}{1-k'^2}\left[-\frac{2k'V_{\rm dc}}{\pi\sqrt{2L_p}}\sin(\theta_p-\theta_s)\right. \\ \quad \left.+\frac{\omega_s}{2}\Psi_s - \frac{k'\omega_p}{2}\Psi_p\cos(\theta_p-\theta_s) + \frac{k'R_p}{2L_p}\Psi_p\sin(\theta_p-\theta_s)\right] \end{cases} \tag{A1}$$

$$\begin{cases} \frac{d\psi_p}{dt} = \frac{1}{\Psi_p}\frac{d\Psi_p}{dt}\psi_p + j\left(\omega+\frac{d\theta_p}{dt}\right)\psi_p \\ \frac{d\psi_s}{dt} = \frac{1}{\Psi_s}\frac{d\Psi_s}{dt}\psi_s + j\left(\omega+\frac{d\theta_s}{dt}\right)\psi_s. \end{cases} \tag{A2}$$

REFERENCES

[1] DigiCert Inc., *Drone Industry Insights*, Sep. 12, 2022. [Online]. Available: https://droneii.com/product/drone-market-report

[2] W. Han, K. T. Chau, C. Jiang, W. Liu, and W. H. Lam, "Design and analysis of quasi-omnidirectional dynamic wireless power transfer for fly-and-charge," *IEEE Trans. Magn.*, vol. 55, no. 7, Jul. 2019, Art. no. 8001709.

[3] S. Wu, C. Cai, X. Liu, W. Chai, and S. Yang, "Compact and free-positioning omnidirectional wireless power transfer system for unmanned aerial vehicle charging applications," *IEEE Trans. Power Electron.*, vol. 37, no. 8, pp. 8790–8794, Aug. 2022.

[4] K. Chen and Z. Zhang, "In-flight wireless charging: A promising application-oriented charging technique for drones," *IEEE Ind. Electron. Mag.*, to be published, doi: 10.1109/MIE.2023.3246236.

[5] Z. Zhang, S. Shen, Z. Liang, S. H. K. Eder, and R. Kennel, "Dynamic-balancing robust current control for wireless drone-in-flight charging," *IEEE Trans. Power Electron.*, vol. 37, no. 3, pp. 3626–3635, Mar. 2022.

[6] Z. Yuan, M. Saeedifard, C. Cai, Q. Yang, P. Zhang, and H. Lin, "A misalignment tolerant design for a dual-coupled LCC-S-compensated WPT system with load-independent CC output," *IEEE Trans. Power Electron.*, vol. 37, no. 6, pp. 7480–7492, Jun. 2022.

[7] A. Hossain, P. Darvish, S. Mekhilef, K. S. Tey, and C. W. Tong, "A new coil structure of dual transmitters and dual receivers with integrated decoupling coils for increasing power transfer & misalignment tolerance of wireless EV charging system," *IEEE Trans. Ind. Electron.*, vol. 69, no. 8, pp. 7869–7878, Aug. 2022.

[8] Y. Gu, J. Wang, Z. Liang, and Z. Zhang, "Mutual-inductance-dynamic-predicted constant current control of LCC-P compensation network for drone wireless in-flight charging," *IEEE Trans. Ind. Electron.*, vol. 69, no. 12, pp. 12710–12719, Dec. 2022.

[9] Y. Lim, H. Tang, S. Lim, and J. Park, "An adaptive impedance-matching network based on a novel capacitor matrix for wireless power transfer," *IEEE Trans. Power Electron.*, vol. 29, no. 8, pp. 4403–4413, Aug. 2014.

[10] S. Assawaworrarit, X. Yu, and S. Fan, "Robust wireless power transfer using a nonlinear parity-time-symmetric circuit," *Nature*, vol. 546, no. 7658, pp. 387–390, Jun. 2017.

[11] Z. Hua, K. T. Chau, W. Liu, and X. Tian, "Pulse frequency modulation for parity-time-symmetric wireless power transfer system," *IEEE Trans. Magn.*, vol. 58, no. 8, Aug. 2022, Art. no. 8002005.

[12] W. X. Zhong, C. Zhang, X. Liu, and S. Y. R. Hui, "A methodology for making a three-coil wireless power transfer system more energy efficient than a two-coil counterpart for extended transfer distance," *IEEE Trans. Power Electron.*, vol. 30, no. 2, pp. 933–942, Feb. 2015.

[13] X. Shu, B. Zhang, Z. Wei, C. Rong, and S. Sun, "Extended-distance wireless power transfer system with constant output power and transfer efficiency based on parity-time-symmetric principle," *IEEE Trans. Power Electron.*, vol. 36, no. 8, pp. 8861–8871, Aug. 2021.

[14] M. Wang, J. Feng, Y. Shi, and M. Shen, "Demagnetization weakening and magnetic field concentration with ferrite core characterization for efficient wireless power transfer," *IEEE Trans. Ind. Electron.*, vol. 66, no. 3, pp. 1842–1851, Mar. 2019.

[15] W. Dong, C. Li, H. Zhang, and L. Ding, "Wireless power transfer based on current non-linear PT-symmetry principle," *IET Power Electron.*, vol. 12, no. 7, pp. 1783–1791, Jun. 2019.

[16] S. Li, S. Lu, and C. C. Mi, "Revolution of electric vehicle charging technologies accelerated by wide bandgap devices," *Proc. IEEE*, vol. 109, no. 6, pp. 985–1003, Jun. 2021.

[17] Y. Wang, T. Li, M. Zeng, J. Mai, P. Gu, and D. Xu, "An underwater simultaneous wireless power and data transfer system for AUV with high-rate full-duplex communication," *IEEE Trans. Power Electron.*, vol. 38, no. 1, pp. 619–633, Jan. 2023.

[18] J.-Q. Zhu, Y.-L. Ban, R.-M. Xu, and C. C. Mi, "An NFC-connected coupler using IPT-CPT-combined wireless charging for metal-cover smartphone applications," *IEEE Trans. Power Electron.*, vol. 36, no. 6, pp. 6323–6338, Jun. 2021.

[19] Y. Gu, J. Wang, Z. Liang, Y. Wu, C. Cecati, and Z. Zhang, "Single-transmitter multiple-pickup wireless power transfer: Advantages, challenges, and corresponding technical solutions," *IEEE Ind. Electron. Mag.*, vol. 14, no. 4, pp. 123–135, Dec. 2020.

[20] H. A. Haus, *Waves and Fields in Optoelectronics*. Englewood Cliffs, NJ, USA: Prentice-Hall, 1984.

[21] J. A. Sanders, F. Verhulst, and J. A. Murdock, *Averaging Methods in Nonlinear Dynamical Systems*, 2nd ed. New York, NY, USA: Springer, 2007.

[22] J. Zhou, B. Zhang, W. Xiao, D. Qiu, and Y. Chen, "Nonlinear parity-time-symmetric model for constant efficiency wireless power transfer: Application to a drone-in-flight wireless charging platform," *IEEE Trans. Ind. Electron.*, vol. 66, no. 5, pp. 4097–4107, May 2019.

[23] J. Wang, R. Chen, C. Cai, J. Zhang, and C. Wang, "An onboard magnetic integration-based WPT system for UAV misalignment-tolerant charging with constant current output," *IEEE Trans. Transp. Electrific.*, vol. 9, no. 1, pp. 1973–1984, Mar. 2023.

[24] Z. Li, J. He, Y. Huo, M. Ban, Y. Liu, and J. Liu, "High-misalignment tolerance and output adjustable wireless charging system via detuned series-series compensated reconfigurable transmission channels," *IEEE Trans. Power Electron.*, to be published, doi: 10.1109/TPEL.2023.3281721.

[25] P. Cao et al., "Embedded lightweight squirrel-cage receiver coil for drone misalignment-tolerant wireless charging," *IEEE Trans. Power Electron.*, vol. 38, no. 3, pp. 2884–2888, Mar. 2023.

Yu Gu (Student Member, IEEE) was born in Shanxi, China, in 1997. He received the B.Eng. degree in automation, in 2018, from Tianjin University, Tianjin, China, where he is currently working toward the Ph.D. degree in control science and engineering.

His research interests include wireless power transfer and power electronic control.

Jiang Wang (Member, IEEE) received the B.Eng., M.Eng., and Ph.D. degrees in electrical engineering from Tianjin University, Tianjin, China, in 1986, 1989, and 1996, respectively.

He is currently a Full Professor with Tianjin University. He has authored four books and 200 peer-reviewed papers. His research interests include nonlinear control, brain-inspired computing, deep learning, data mining, industrial control, etc.

Zhenyan Liang (Member, IEEE) received the B.Eng. degree in thermal energy and power engineering from Shanghai Jiao Tong University, Shanghai, China, in 2004, and the M.S. degree in control science and engineering, in 2019 from Tianjin University, Tianjin, China, where she is currently working toward the Ph.D. degree in control science and engineering.

Her research interests include wireless power transfer and predictive control for electrical drives.

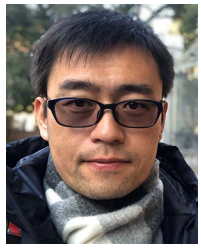

Zhen Zhang (Senior Member, IEEE) received the B.Eng. and M.Eng. degrees in automation from Tianjin University, Tianjin, China, in 2004 and 2007, respectively, and the Ph.D. degree in electrical engineering from The University of Hong Kong, Hong Kong, in 2014.

In 2014, he was a Visiting Scholar with the IBM Research Laboratory supported by IBM Global Great Minds Program. Then, he served as a Postdoctoral Fellow with The University of Hong Kong. He is currently a Professor of electrical engineering with the School of Electrical and Information Engineering, Tianjin University, and an Honorary Associate Professor with the Department of Electrical and Electronic Engineering, The University of Hong Kong. He has authored and coauthored more than 60 internationally refereed papers as well as two books published by Wiley-IEEE Press and Cambridge University Press, respectively. His current research focuses on the advanced control for power conversion with emphasis on wireless power transfer and motor drives.

Dr. Zhang is currently the Chair of the IEEE Beijing Section IES Chapter and an Associate Editor for the IEEE TRANSACTIONS ON INDUSTRIAL ELECTRONICS, IEEE TRANSACTIONS ON INDUSTRIAL INFORMATICS, and IEEE INDUSTRIAL ELECTRONICS MAGAZINE. He was the recipient of the Humboldt Research Fellowship, Carl Friedrich von Siemens Research Fellowship, Japan Society for the Promotion of Science Visiting Fellowship, 2020 Best Paper Award for IEEE TRANSACTIONS ON INDUSTRIAL ELECTRONICS, and IEEE J. David Irwin Early Career Award.